JOURNAL OF MATERIALS SCIENCE **34** (1999) 7–20

Atomistic simulation of chemical vapor deposition of (111)-oriented diamond film using a kinetic Monte Carlo method

M. GRUJICIC, S. G. LAI
Department of Mechanical Engineering, 241 Flour Daniel Building, Clemson University, Clemson, SC 29634-0921

Chemical vapor deposition (CVD) of (111)-oriented diamond film is modeled using a kinetic Monte Carlo atomic scale method. The method is parameterized by the rates of the accompanying surface chemical reactions and permits one of these reactions to take place at each simulation step. The effect of local surface structure and morphology on the rates of surface reaction is examined. Film growth at two different chemical compositions of the feed gas and two substrate temperatures is studied in order to determine the effect of these process parameters on (a) the quality of the deposed film and (b) the rate of deposition. The quality of the film is judged by concentration of the point defects (vacancies and H atoms embedded in the film) and by surface roughness. The results obtained show that the parameters that increase the deposition rate, primarily the substrate temperature and the concentration of CH_4 in the feed gas, also increase the defect content and surface roughness.

1. Introduction

The CVD of diamond from a precursor gas mixture containing a small amount of hydrocarbon (usually methane CH_4, acetylene C_2H_2, and so on) in hydrogen at subambient pressures (typically 1–200 torr) has become commercially viable over the last decade [1–3]. The gas mixture is typically heated using hot filaments, plasmas, combustion flames, and other means to promote the dissociation of some of the molecular hydrogen, H_2, into atomic hydrogen, H, and formation of various hydrocarbon radicals. Although under standard CVD processing conditions graphite is the stable form of carbon, H atoms bond with the surface carbon atoms and passivate it by converting the graphite-type sp^2-bonded surface C atoms into the sp^3-bonded diamond-type C atoms [2, 3]. Whereas it is well-established that deposition of diamond occurs by the incorporation of chemisorbed hydrocarbon radicals, the details of the diamond growth mechanism are still not well-understood. This is primarily caused by the fact that the atomic-scale events that lead to diamond growth are difficult to study *in situ*. Hence, the current understanding of diamond growth has been primarily gained through the use of computer modeling and simulations or from the interpretation of *ex situ* experimental data, or both.

There are several different modeling approaches used to analyse diamond growth process. Calculations of the surface energetics are primarily used to determine kinetic parameters of individual surface reactions [4–7] and examine the stability of various surface configurations [8–14]. Several one-dimensional models have been developed to analyse the deposition of diamond, but they fail to incorporate the effects of surface morphology and local atomic configuration on the growth process [15–18]. Molecular dynamics simulations are used to model the deposition of diamond films but only over a millisecond of growth time [19]. Recently, Dawnkaski et al. [20] and Battaile *et al.* [21] carried out three-dimensional atomic-scale simulations of the (100) and (111) diamond surface growth, respectively.

In the present work, the three-dimensional atomistic simulation method for CVD proposed by Battaile *et al.* [22] is used to study the (111) growth of diamond. This method allows the effects of surface chemistry, local atomic coordination, and surface structure to be incorporated into simulation and is capable of simulating hours of the deposition process under commonly used processing conditions. The original model of Battaile *et al.* [22] has been further developed in the present work to take into account the fact that the rate of the same chemical reaction is dependent on whether the reaction takes place at the step edges or on the surface terraces.

The organization of the paper is as follows: In section 2.1, the procedures used to construct the diamond lattice and the (111) substrate are discussed. Basic kinetics of surface reactions and a brief overview of the kinetic Monte Carlo method are presented in sections 2.2 and 2.3, respectively. The results obtained in the present work are shown and discussed in section 3. Main findings resulting from the present study are summarized in section 4.

2. Procedure

2.1. Generation of diamond lattice and (111) substrate

The growth of diamond film by CVD has been simulated using a rigid diamond-type lattice. In other words, the atomic relaxations and vibrations are not considered. The orientation of the lattice is defined as $x = [11\bar{2}]$, $y = [1\bar{1}0]$, and $z = [111]$. The film is allowed to grow in z direction; the periodic boundary conditions are applied in the x and y directions in order to avoid the film edge effects. The size of the computational lattice in the x–y plane is $90\, d_{(112)} \times 40\, d_{(110)}$, where $d_{(uvw)}$ is the spacing of the (uvw) diamond planes. Initially, six (111) planes of the diamond lattice are filled with carbon atoms to form a substrate six layers thick. To passivate the top layer of the substrate, the substrate is terminated with a layer of atomic H. A small segment of the substrate is shown in Fig. 1.

The growth of diamond requires that the H-terminated substrate surface be activated, which can take place by either desorption or abstraction of the chemisorbed atomic H. Once a substrate surface site is activated, it can be repassivated by chemisorption of either an atomic H or a hydrocarbon molecule. The chemisorbed hydrocarbon molecule can desorb and thus reactivate the site. Conversely, the hydrocarbon molecule may take part in one of the possible surface reactions that leads to the incorporation of carbon atom from the hydrocarbon molecule into the diamond lattice and thus to film growth.

The film deposition is simulated by allowing the substrate to interact with a hot filament–heated process gas containing various concentrations of H, H_2, CH_3, and C_2H_2 in accordance with the set of surface chemical reactions reported by Battaile *et al*. [22] (Table I).

2.2. Surface reaction kinetics

The kinetics of surface reactions is represented using the general formalism as used in the Surface ChemKin computer program [23]. Within this formalism, the forward rate constant for reaction i, k_{f_i}, is assumed to be given by the following Arrhenius-type relation:

$$k_{f_i} = A_i T^{\beta_i} \exp\left(-\frac{E_i}{RT}\right), \tag{1}$$

where the pre-exponential factor A_i, the temperature exponent β_i, and the activation energy E_i for all the surface reactions considered here (listed in Table I), R is the universal gas constant, and T is the absolute temperature. A schematic of the atomic rearrangements accompanying the surface reactions treated in the present work is given in Fig. 2. The dashed lines are used in Fig. 2 to indicate the location of the surface. It should be noted that the atomic rearrangement accompanying the reaction shown in the second column of Fig. 2 pertains to when that reaction takes place on surface terraces; the atomic rearrangement shown in the third column corresponds to when the same chemical reaction takes place at surface steps.

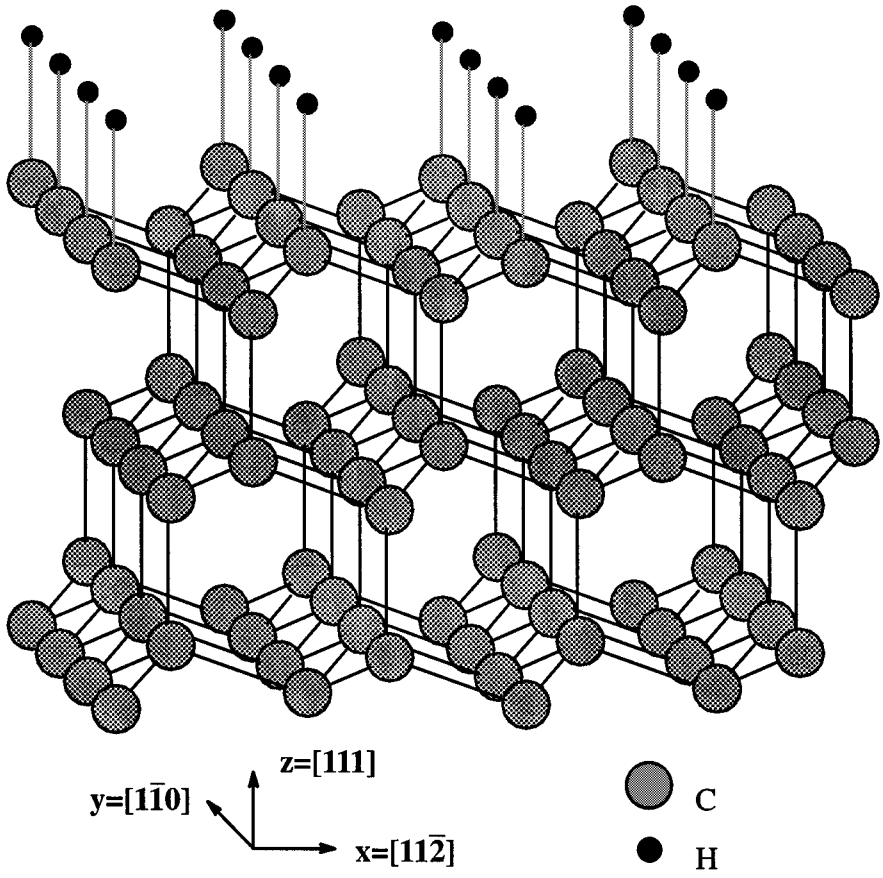

Figure 1 A section of the diamond substrate for chemical vapor deposition of a diamond film. Diamond atoms are represented by open circles and hydrogen atoms by filled circles.

TABLE I Reaction rate coefficients for the chemical reactions accompanying CVD of diamond as reported. 3–5 A is in units of mol, cm^3, and s; E and ΔH are in units of kcal/mol; and ΔS is in units of cal/(mol · K). C_d—surface diamond atom, *—surface biradical

	Reaction	A	n	E	ΔH	ΔS
1	$C_dH + H \leftrightarrow C_d + H_2$	1.3×10^{14}	0	7.3	−9.9	5.3
2	$C_d + H \leftrightarrow C_dH$	1.0×10^{13}	0	0.0	−96.9	−32.8
3	$C_dCH_2 + H \leftrightarrow C_d + CH_3$	3.0×10^{13}	0	0.0	−24.6	7.9
4	$C_d + CH_3 \leftrightarrow C_dCH_3$	5.0×10^{12}	0	0.0	−70.9	−42.0
5	$C_d + C_2H_2 \leftrightarrow C_dC_2H_2$	8.0×10^{10}	0	7.7	−19.0	−10.7
6	$C_dCH_y + H \leftrightarrow C_dCH_{y-1} + H_2$	2.8×10^{7}	2	7.7	−11.3	6.6
7	$C_dCH_y + H \leftrightarrow C_dCH_{y+1}$	1.0×10^{13}	0	0.0	−83.0	−34.1
8	$C_dC_2H_y + H \leftrightarrow C_dC_2H_{y-1} + H_2$	9.0×10^{6}	2	5.0	−8.9	8.7
9	$C_dC_2H_y + H \leftrightarrow C_dC_2H_{y+1}$	2.0×10^{13}	0	0.0	−47.7	−36.2
10	$C_dCH_y + CH_3 \rightarrow C_dC_2H_{y+3}$	5.0×10^{12}	0	0.0	—	—
11	C_d–$C_d \leftrightarrow C_d + * + C_d$	1.0×10^{13}	0	0.0	4.9	0.4
12	$C_d + * + C_dC_xH_y \rightarrow C_d + C_dC_{x-1}H_y + C_d$	2.0×10^{13}	0	8.8	—	—

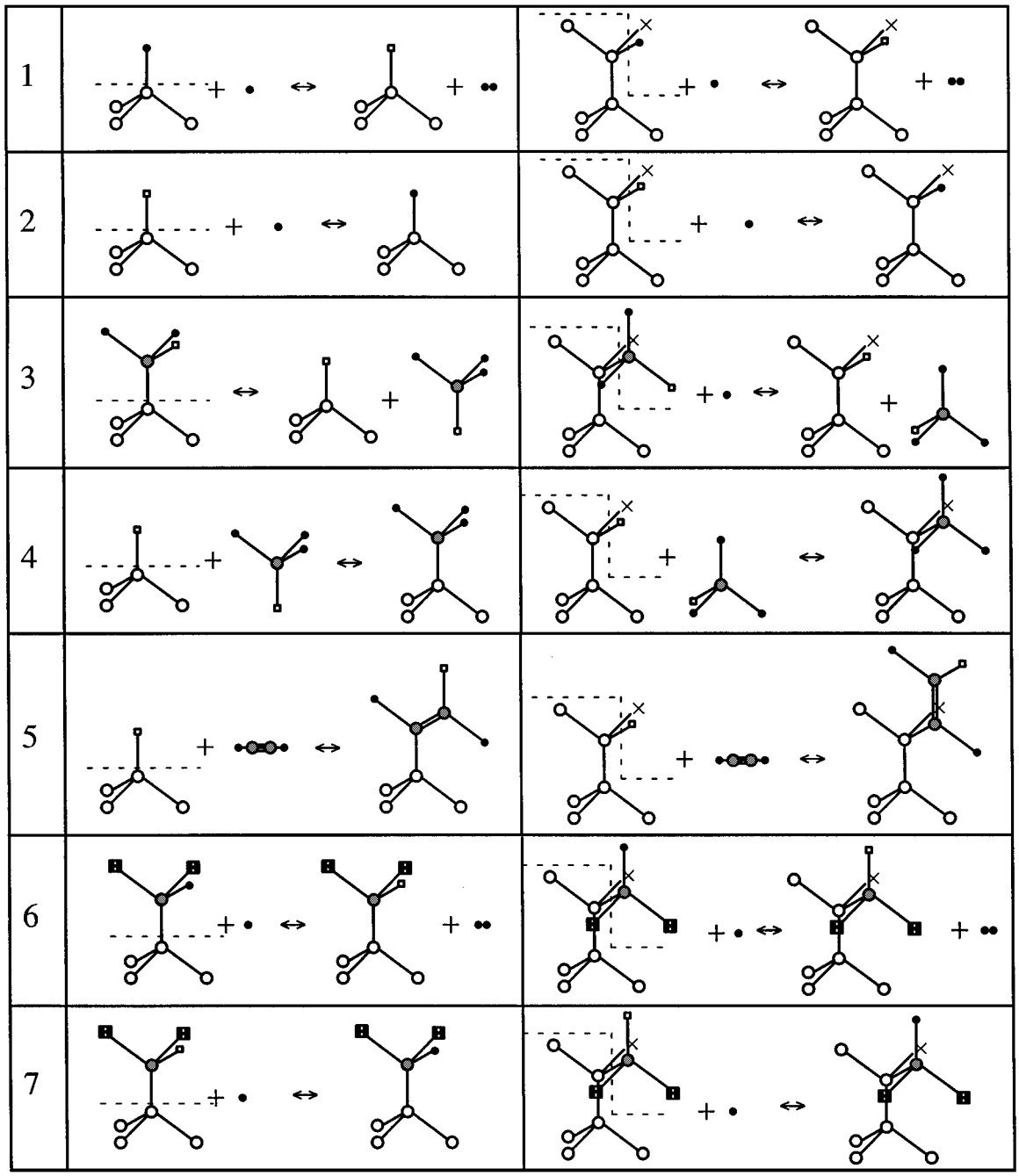

Figure 2 Atomic rearrangements accompanying each of the 12 surface reactions listed in Table 1. The reaction number is given in the first column. The dashed line indicates the location of the film surface.

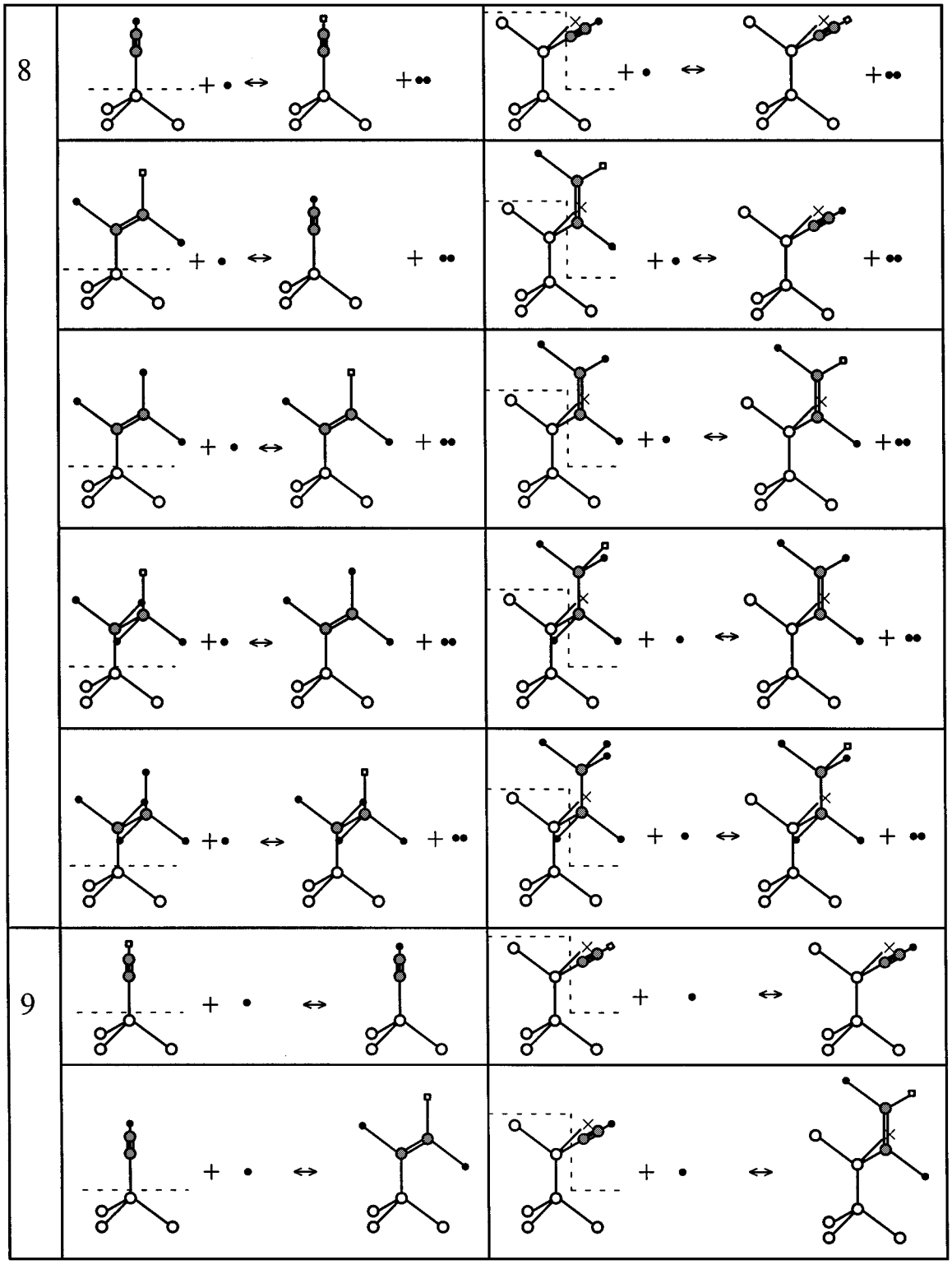

Figure 2 (*Continued*).

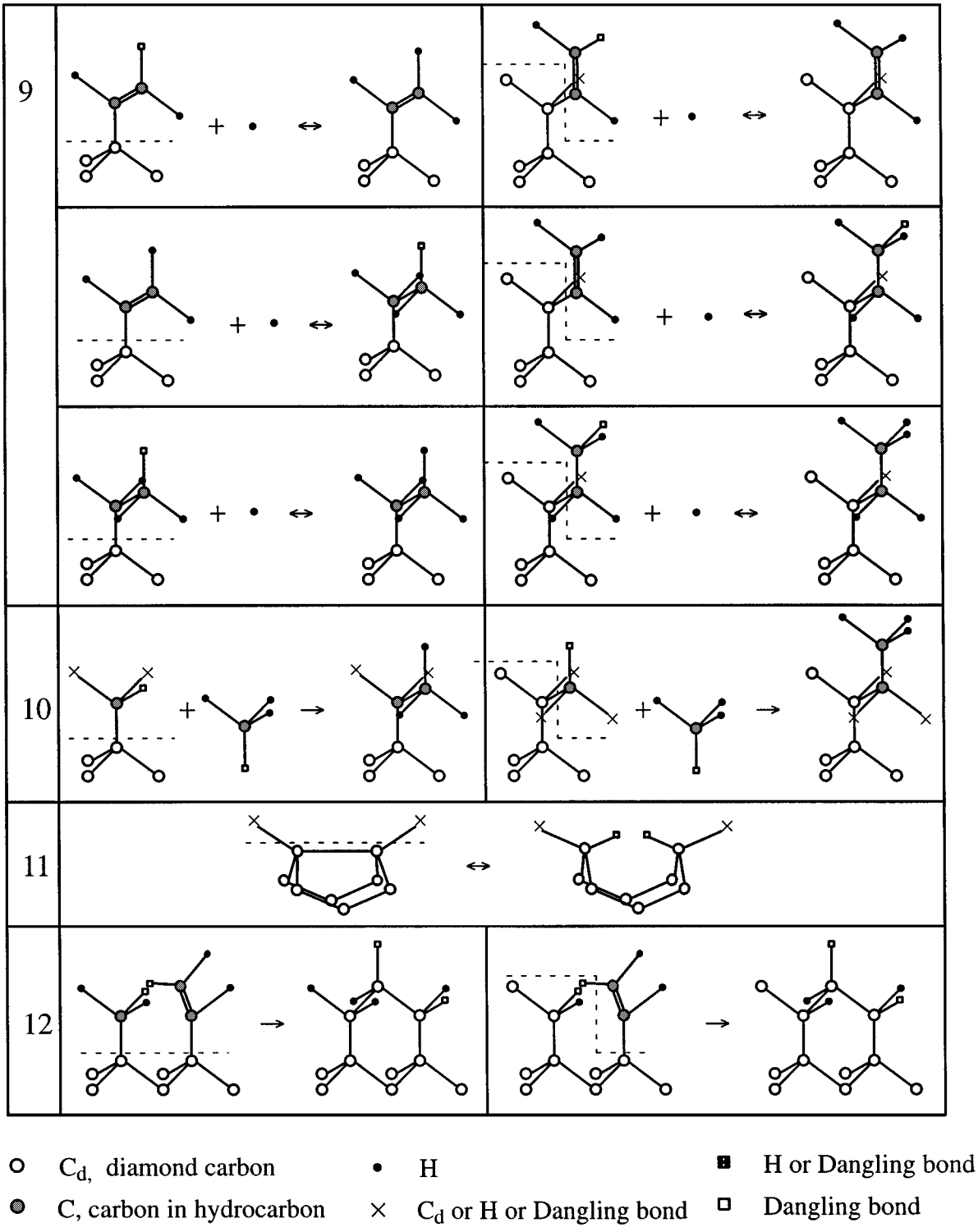

Figure 2 (*Continued*).

The reverse reaction rate constant is related to the forward reaction rate constant via the following equation:

$$k_{r_i} = \frac{k_{f_i}}{K_{C_i}}, \tag{2}$$

where K_{C_i} is the equilibrium constant expressed in concentration units and is related to the equilibrium constant expressed in pressure units, K_{P_i} as

$$K_{P_i} = K_{C_i}\left(\frac{P_{\text{atm}}}{RT}\right)^{-\sum_{k=1}^{K_g} v_{ki}} \prod_{n=N_s^f}^{N_s^1} \left(\Gamma_n^0\right)^{-\sum_{k=K_s^f(n)}^{K_s^l(n)} v_{ki}} \times \prod_{k=K_s^f(n)}^{K_s^l(n)} \sigma_k^{v_{ki}} \tag{3}$$

where P_{atm} is the pressure of 1 atm; Γ_n^0 the standard state density of the surface sites of type n; $\sigma_k(n)$ the number of sites of type n occupied by species k; V_{ki}s are the stoichiometric reaction coefficients associated with species k and reaction i; K_g the total number of gas species; $K_s^f(n)$ and $K_s^l(n)$ the first and the last surface species residing on n-type sites, respectively; and N_s^f and N_s^l the first and the last surface site types, respectively.

K_{P_i} can be computed from the standard state enthalpy change ΔH_i^0 and the standard state entropy change ΔS_i^0 accompanying reaction i as

$$K_{P_i} = \exp\left(\frac{\Delta S_i^0}{R} - \frac{\Delta H_i^0}{RT}\right) \tag{4}$$

ΔH_i^0 and ΔS_i^0 for the set of surface reactions used in the present work are listed in Table I.

For the reactions, 1, 3, 6, 8, 11, and 12 listed in Table I, the sum

$$\sum_{k=1}^{K_g} v_{ki} = 0 \text{ and hence } \left(\frac{P_{\text{atm}}}{RT}\right)^{\sum_{k=1}^{K_g} v_{ki}} = 1.$$

For the remaining reactions listed in Table I (reactions 2, 4, 5, 7, 9, and 10) the sum

$$\sum_{k=1}^{K_g} v_{ki} = -1 \text{ and hence } \left(\frac{P_{\text{atm}}}{RT}\right)^{\sum_{k=1}^{K_g} v_{ki}} = 0.0122\frac{K}{\text{cm}^3} \times \frac{1}{T}.$$

As mentioned earlier, the rate of each reaction is allowed to depend on whether the reaction takes place at surface steps or on surface terraces. To obtain the ratio of the reaction rate constants for a reaction taking place at surface steps and for the same reaction taking place on surface terraces, the energetics of the two modes of reaction are determined using the molecular statics method [25]. This approach is demonstrated by applying it to reaction 12.

Fig. 3a shows the atomic configuration corresponding to the unreacted state of reaction 12 for when this reaction takes place on surface terraces. The potential energy of this configuration is minimized relative to

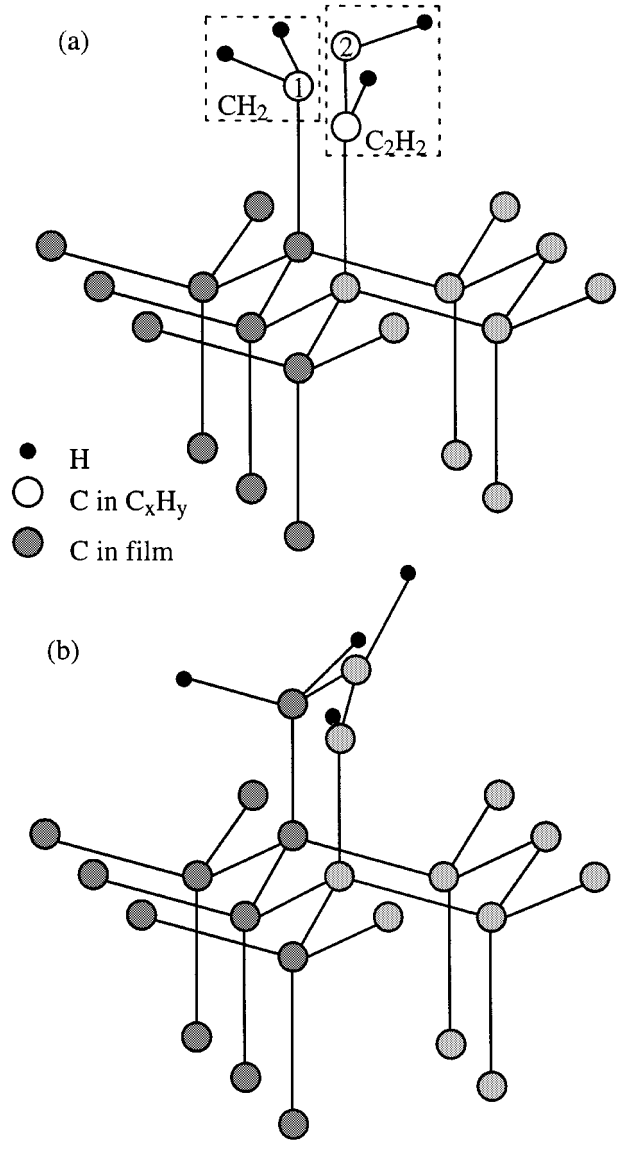

Figure 3 Equilibrated atomic configurations of (a) the initial (unreacted) and (b) the final (reacted) states associated with reaction 12 taking place on surface terraces.

the spatial coordinates of the atoms using the conjugate gradient method [26]. The atomic interactions are quantified using the interatomic potential developed by Brenner [4]. The Brenner potential accounts for both intramolecular chemical bonding in a wide range of hydrocarbon molecules as well as carbon–carbon bonding and defect energies in diamond and graphite. The potential is based on the bond order formalism and includes the corrections for non-local effects, inherent overbinding of radicals and conjugation of the carbon–carbon bonds. Fig. 3b shows the atomic configuration after energy minimization associated with the reacted state of reaction 12 when this reaction takes place on surface terraces. The main feature of reaction 12 is formation of the C–C bond between carbon atoms marked 1 and 2. Since the distance between the two carbon atoms changes by less than 20% between the unreacted and the reacted states, a unique reaction path is defined in the following way. The trajectory of each of the two carbon atoms between their initial (unreacted) and final (reacted) positions is assumed to be straight line. The two atoms are next displaced along their trajectory

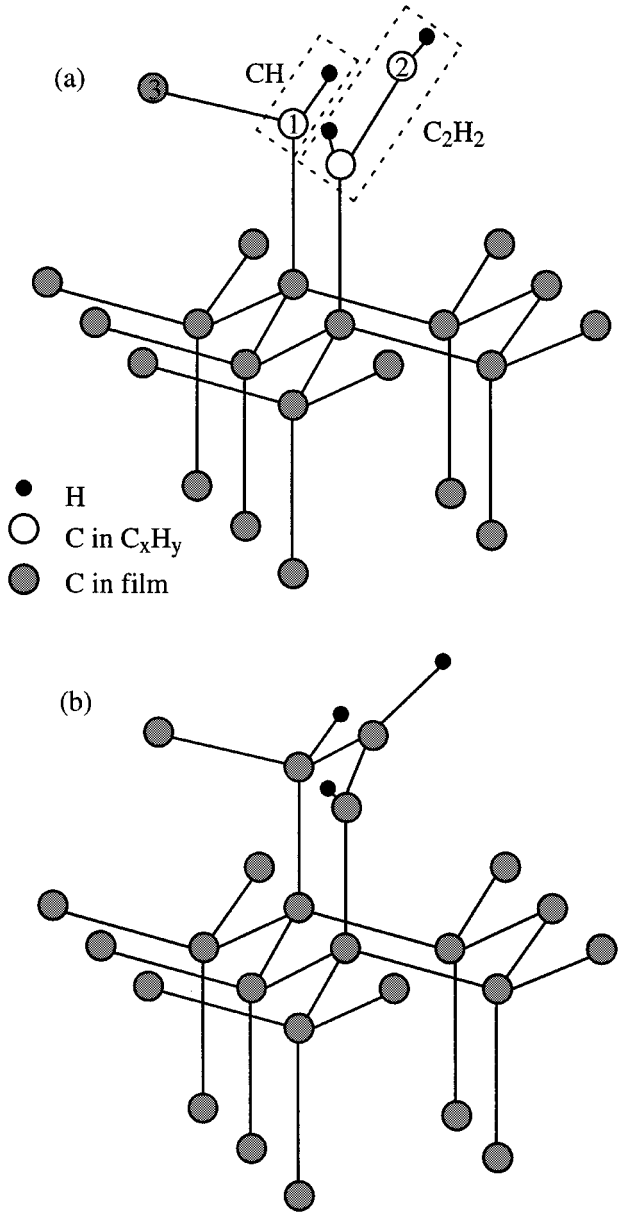

Figure 4 Equilibrated atomic configurations of (a) the initial (unreacted) and (b) the final (reacted) states associated with reaction 12 taking place at surface steps.

in equal increments (normalized relative to the total displacement of the carbon atom in question) and the potential energy minimized relative to the position of the remaining atoms in the system. The initial and the final atomic configurations for reaction 12 taking place at surface steps are shown in Fig. 4a and b, respectively. In this case, the reaction is considered to take place in two steps: (a) hydrogen abstraction from CH_2 and the formation of a C–C bond between the carbon atoms marked 1 and 3 and (b) formation of a C–C bond between the carbon atoms marked 1 and 2.

The variation of the potential energy along this reaction path for reaction 12 taking place both on surface terraces and at surface steps is shown in Fig. 5. The results shown in Fig. 5 are used to determine the force constants (a^{terr} and a^{step}) proportional to the curvature of the energy versus reaction path curve at the initial (unreacted) state and the activation energies (E^{terr} and E^{step}) for the two modes of reaction 12. The ratio of the reaction rate constants of the terrace mode and of the step mode of each of the reactions listed in Table I is calculated as

$$R_{\text{rxn}} = \left(\frac{a^{\text{terr}}}{a^{\text{step}}}\right)^{\frac{1}{2}} \exp\left(-(E^{\text{terr}} - E^{\text{step}})/RT\right) \quad (5)$$

This procedure yields a value of $R_{\text{rxn}} = 3.2$ for reaction 12.

2.3. Kinetic Monte Carlo method

The temporal evolution of the diamond film during growth is simulated using the version of the kinetic Monte Carlo method recently developed by Battaile *et al*. [22]. Within this method, one surface reaction is allowed to take place at one surface site during each time step. The occurrence of one of the reactions at one of the sites is termed an event. At each time step, a list of all possible events is constructed, and the probability for each event is set proportional to the rate of the associated surface reaction relative to the rates of the surface reactions associated with all the other possible events. In other words, at each time step, a random number α uniformly distributed in the range (0, 1) is generated to select the event m from M possible events in accordance with the relation

$$\sum_{j=0}^{m-1} r_j \Big/ \sum_{j=0}^{M} r_j < \alpha < \sum_{j=0}^{m} r_j \Big/ \sum_{j=0}^{M} r_j \quad (6)$$

r_j in Equation 6 is the rate of surface reaction associated with event j, and $r_0 = 0$.

After an event has occurred, the total number of possible events M and the sequence in which the events are listed are updated and the aforementioned procedure is repeated.

The Monte Carlo method used in the present work uses a variable time step to account for the fact that different events take place at different rates. At each simulation step the time increment Δt is computed as

$$\Delta t = -\ln(\beta) \Big/ \sum_{i=1}^{M} r_i, \quad (7)$$

where β is a random number uniformly distributed in the range (0, 1), and the denominator in Equation 7 represents the sum of the reaction rates of all the events that can occur at the given simulation step.

The time increment given by Equation 7 is adjusted dynamically and stochastically to accommodate the fastest possible event at each simulation step, greatly reducing restrictions associated with the conventional fixed time increment methods. In other words, when fast reactions are possible in a given step, the denominator in Equation 7 is large and Δt is small (i.e. the time scale is fine). Conversely, when only show reactions are possible at a given simulation step, the time increment is large (i.e., the time scale is coarse).

3. Results

3.1. Qualitative analysis of various stages of deposition

The atomic structure of the (111) diamond surface at three different stages of deposition under the CVD

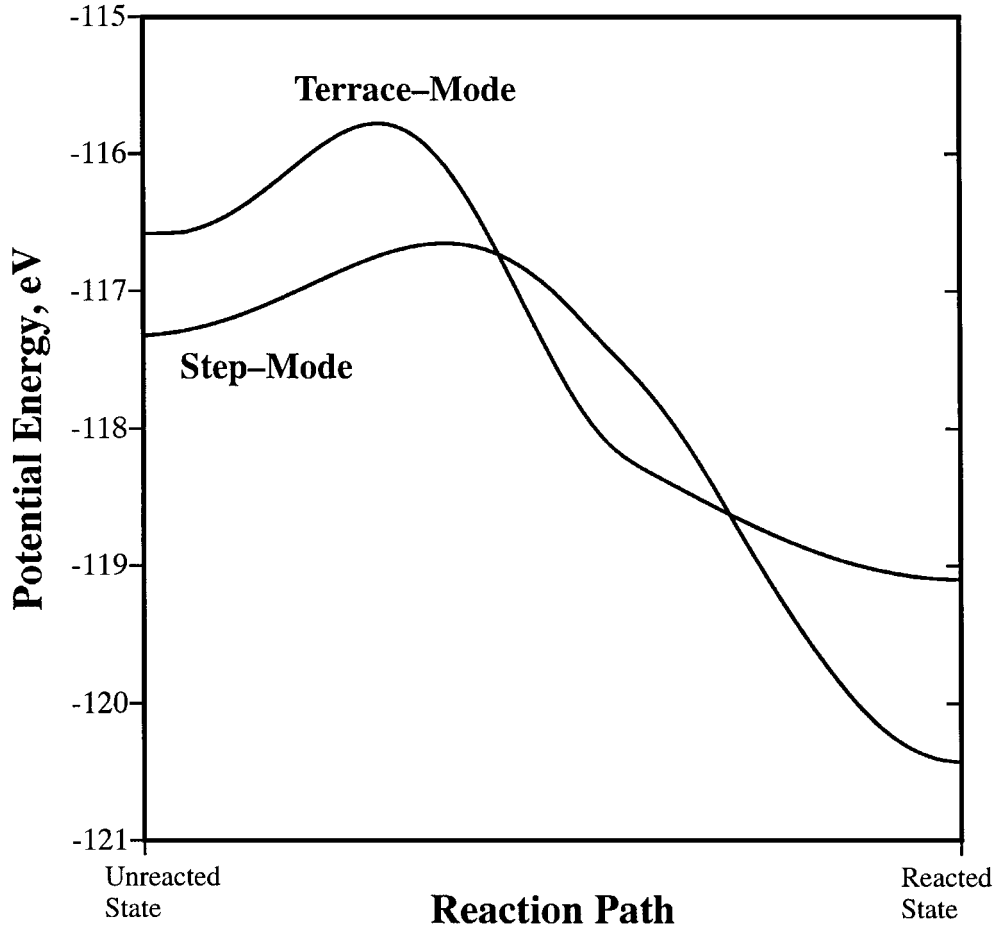

Figure 5 Variation of the potential energy along the reaction path for reaction 12 taking place on surface terraces and at surface steps.

conditions typical for a hot filament reactor—the feed gas consisting of 0.9% CH_4, 7% Ar, and 92.1% H_2 and the gas temperature equal to 1720 K and the substrate temperature equal to 1500 K—are shown in Fig. 6. At short simulation times, the atomic surface structure is dominated by isolated islands of new (111) layers formed on the initially atomically flat substrate surface (Fig. 6a). As the deposition process proceeds, film growth enters the second stage, characterized by the lateral growth of islands (Fig. 6b), which occasionally leads to their coalescence. At long deposition times (Fig. 6c), the atomic structure reaches the state of dynamic equilibrium, in which the existing incomplete (111) layers are being filled by carbon adatoms while new (111) layers are being formed. The details of the dynamics of evolution of the surface atomic structure in the third stage of deposition are discussed in the next section.

3.2. The standard case

In order to establish the effect of process parameters (primarily the concentrations of CH_4 and H_2 in the feed gas and the gas and substrate temperatures) on the atomic surface structure of the diamond film processed by chemical vapor deposition, the case of the feed gas consisting of 0.4% CH_4, 7% Ar, and 92.6% H_2, gas temperature $T_g = 1720$ K, substrate temperature $T_s = 1500$ K, and pressure $P = 20.25$ torr has been termed the standard case (Case I) and considered first.

Case I is first analysed using the SPIN computer program originally developed by Dandy and Coltrin [24] to determine the concentrations (partial pressures) of various species in the gas next to the substrate (film) surface. The program simulates diamond deposition in a hot filament reactor system using the continuum approach to the species and heat transport and to the gas phase and surface reaction kinetics. The configuration analysed consists of a disk-shaped filament mesh heater lying in a plane parallel to a disk-shaped substrate (the heater to substrate distance = 1.3 cm, infinitely large heater and substrate radii) with reaction gases passing through the heater uniformly in the direction perpendicular to the substrate. Under these conditions the following concentrations of the gas species at the gas–substrate interface are obtained: 0.2% H, 88.9% H_2, 0.02% CH_3, and 0.2% C_2H_2.

The top view of the (111) diamond surface and the evolution of its morphology during the deposition process under the aforementioned processing conditions for Case I are shown in Fig. 7. Large circles are used in Fig. 7 (and Fig. 8) to indicate the surface atoms, defined as the atoms with less than four diamond bonds. In other words, these atoms have active bonds that allow them to take part in one of the surface reactions listed in Table I. The atoms represented by dark dots in Fig. 7 (and Fig. 8) correspond to the bulk diamond atoms that have four carbon bonds and, therefore, cannot take part in any surface chemical reactions. To further help the analysis of the surface morphology, different shades of grey are used to designate the relative magnitude of the z coordinate of the atoms. The white (the brightest shade of grey) atoms are located on the very top of

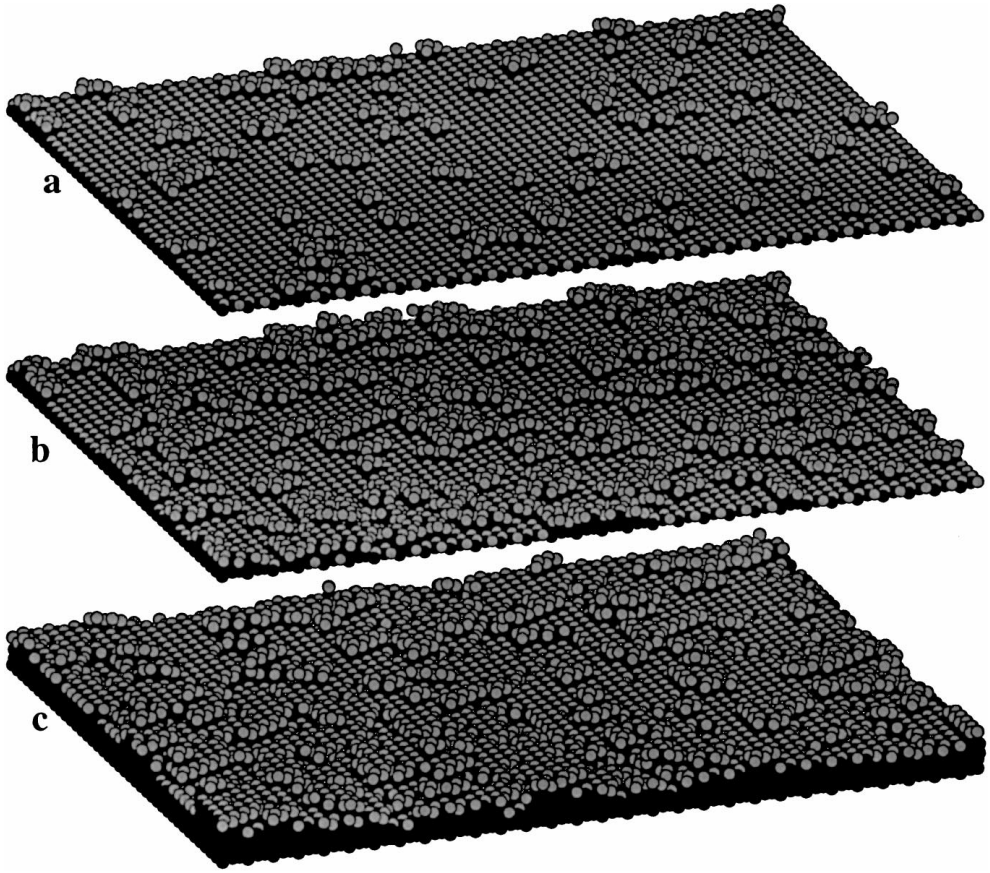

Figure 6 Typical atomic surface structure during CVD of diamond: (a) In the early stages of deposition isolated islands of diamond adatoms dominate surface structure; (b) growth and coalescence of the islands at intermediate stages of deposition, and (c) the surface structure reaches a dynamic equilibrium at longer deposition times.

surface asperities; the black (the darkest shade of grey) ones are located on the bottom of surface valleys. To improve the clarity of the top view of atomic configurations, only the top six to eight (111) planes (depending on the stage of deposition, i.e., the deposition time) are displayed in Fig. 7. Consequently, the hole seen in Fig. 7a does not represent a vacancy in the deposited film but rather pertains to a surface atom located below the top six to eight (111) surface layers.

The atomic surface configuration shown in Fig. 7a corresponds to the third stage of film growth and is obtained after 3.7 s. The top six (111) layers in this configuration are marked using numbers 1 through 6, with layer 1 being on the very top. A close examination of this configuration reveals several important features. A number of islands containing layers 1 and 2 are observed. Some of these islands (A) contain only one atom of layer 1 and two or three atoms of layer 2. The others (B) are significantly larger in size. Layers 3 through 6 are all incomplete, with the extent of completeness increasing with the layer number. In fact, layer 6 is almost completely filled. In order to identify the main events taking place during film deposition, the deposition time is increased in small increments, and the resulting configurations are compared with the one shown in Fig. 7a (the reference configuration).

The surface atomic configuration obtained after 3.8 s (Fig. 7b) shows that several carbon adatoms (F) have been appended to layer 6. As a result, layer 6 becomes completely filled. In addition, because the edges of the incomplete layers act as favorable sites for carbon deposition, layers 3, 4, and 5 have expanded considerably and at several places (D) layers 3 and 4 cover layer 5 almost entirely. Small isolated islands, marked A in Fig. 7a, have undergone a considerable growth in the lateral directions in the 3.7- to 3.8-s time period and are designated as B in Fig. 7b. Meanwhile, only one new island (A) has formed.

The atomic surface configuration obtained after 4.3 s of simulation time is shown in Fig. 7c. Several newly nucleated islands containing layer 1 (A) can be observed. In addition, several pre-existing islands, marked B in Fig. 7b, have grown in the lateral directions. Few such islands (E in Fig. 7c) have extended to the point that they merged with their neighbors. Lower layers have continued to grow (D), and, consequently, layer 5 is approaching the condition of complete filling.

When simulation time reached 4.6 s (Fig. 7d), two new (111) layers (C) started to form via the nucleation of a new island. Since the new (111) layers are on the very top of the surface, they had to be assigned the brightest shades of grey and, consequently, the colors of the previously existing surface layers had to be rescaled. The new layers are designated as 0 and -1. A comparison of Fig. 7b and d shows that the pre-existing layers have continued to grow and merge. The most prominent feature of the configuration shown in Fig. 7d is the presence of a vacancy (V), however. The carbon atom that would normally be present in the center of the tetrahedron centered at V is missing. Further analysis of

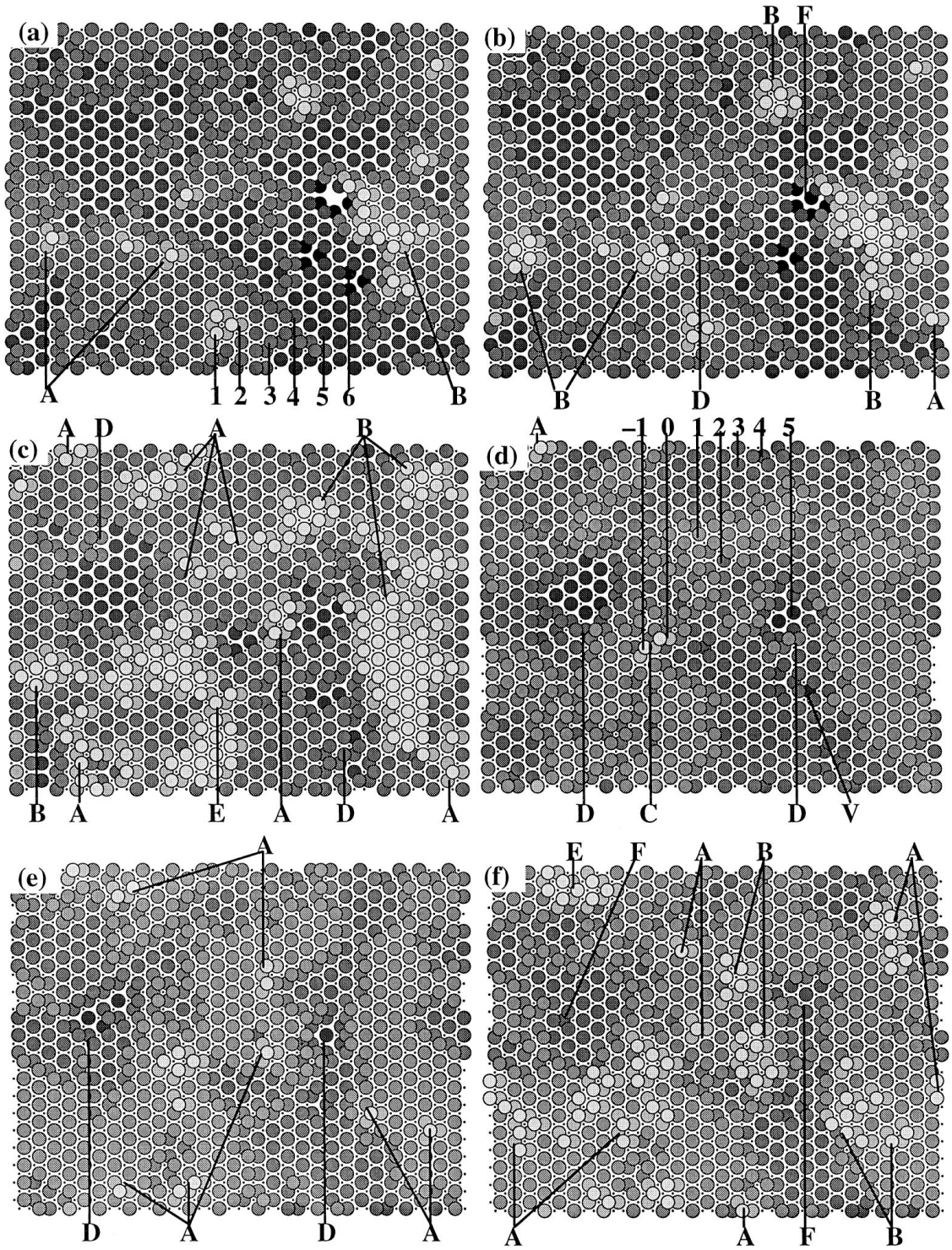

Figure 7 Evolution of the (111) surface morphology in a diamond film during chemical vapor deposition under the following conditions: hot filament reactor; feed gas (0.4% CH_4, 7% Ar, 92.6% H_2, $T_g = 1720$ K), substrate temperature ($T_s = 1500$ K). Deposition times: (a) 3.7 s, (b) 3.8 s, (c) 4.3 s, (d) 4.6 s, (e) 5 s, and (f) 5.3 s.

Fig. 7d reveals that a new island (A) has formed and that the pre-existing layers have continued to grow (D).

The surface atomic configuration after 5 s (Fig. 7e) shows that layers 3, 4, and 5 have continued to grow and approach the state of complete filling (D). In addition, several islands containing layers 0 and -1 (A) have formed on the surface top.

After 5.3 s of deposition time (Fig. 7f), the growth of layer 5 has been completed (F). Several new islands containing layers 0 and -1 (A) have formed. The pre-existing islands (B) have expanded and few of them have merged (E).

In addition to the standard case (Case I), three additional cases were analysed: Case II, 0.4% CH_4, 7% Ar, 92.6% H_2, $T_g = 1720$ K, $T_s = 1073$ K; Case III: 7% CH_4, 7% Ar, 86% H_2, $T_g = 1720$ K, $T_s = 1073$ K; and Case IV: 7% CH_4, 7% Ar, 86% H_2, $T_g = 1720$ K, $T_s = 1500$ K. The four cases allow the effects of the substrate temperature (1073 K versus 1500 K) and the CH_4 concentration in the feed gas (0.4% versus 7%) to be explored.

A close examination of the surface atomic structure and its evolution in the third stage of film deposition for Cases II and III (both with $T_s = 1073$ K) reveals the

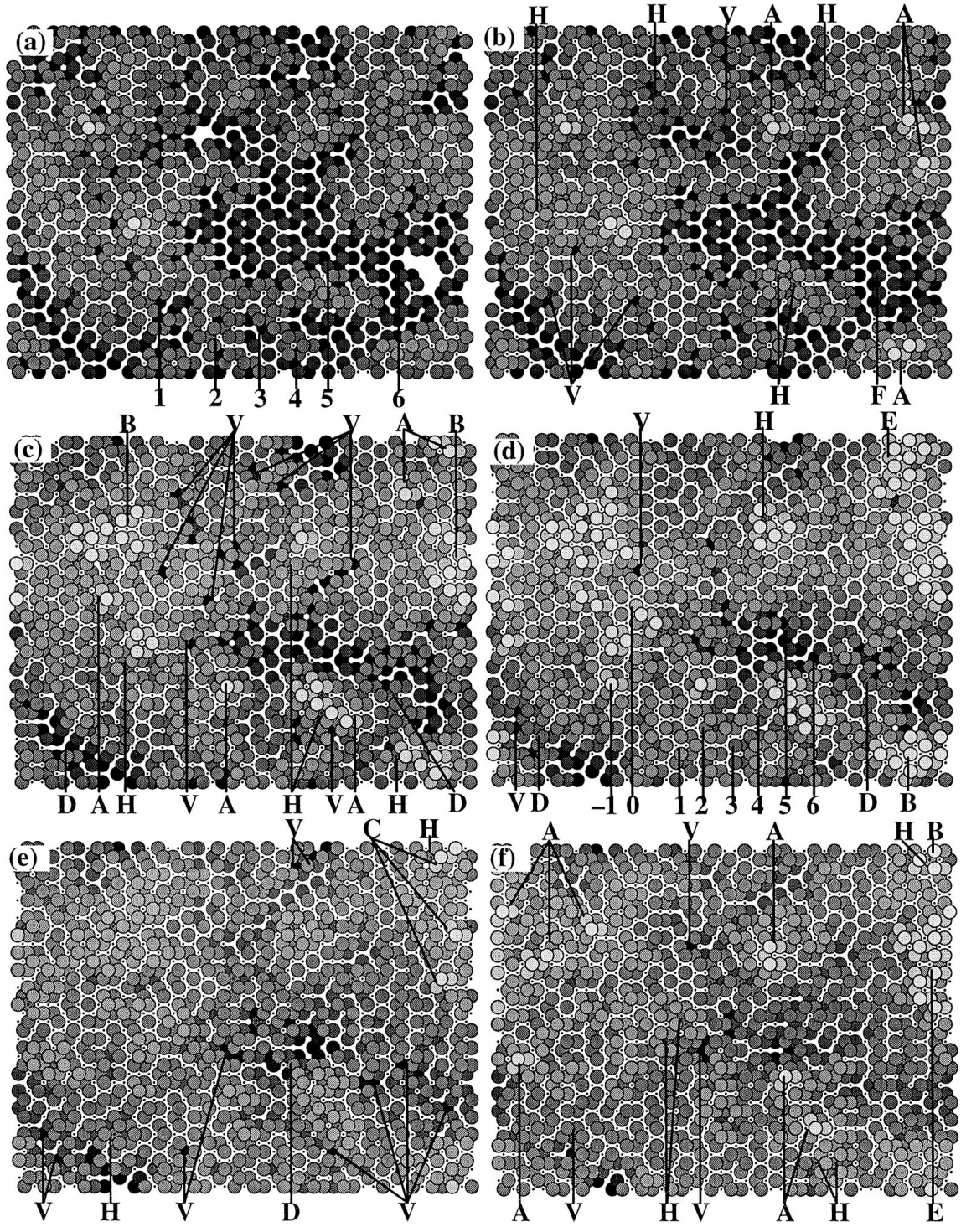

Figure 8 Evolution of the (111) surface morphology in a diamond film during chemical vapor deposition under the following conditions: hot filament reactor; feed gas (7% CH_4, 7% Ar, 86% H_2, $T_g = 1720$ K), substrate temperature ($T_s = 1500$ K). Deposition times: (a) 3.7 s, (b) 3.8 s, (c) 4.3 s, (d) 4.6 s, (e) 5 s, and (f) 5.3 s.

presence of similar morphological features and similar surface deposition events as the ones observed in Case I, and hence the corresponding atomic surface configurations are not shown. An additional new feature is found for Case IV (the high T_s/high CH_4 percentage case), however. In particular, H atoms are found embedded in the diamond film. The evolution of the atomic surface configuration for Case IV at the same deposition times as those for Case I is shown in Fig. 8. To help interpret the atomic surface configurations for Case IV, the top six (111) layers are designated using numbers 1 through 6, and various events marked as following: A, nucleation of a new island; B, lateral growth of the existing islands; C, formation of a new (111) layer; D, filling of the lower (111) layers; E, merging of the islands; F, layer completion; and V, a vacancy. Hydrogen atoms embedded in the film are marked H in Fig. 8 and are characterized by the fact that bulk carbon atoms with four carbon neighbors (represented by dots in Fig. 8) are located above surface carbon atoms with less than four diamond bonds (represented with circles). Careful analysis of the film structure obtained after 10 s revealed the presence of hydrogen atoms embedded in the film for Case III. No such defects are found in Cases I and II. This finding

appears to be related to the fact that the surface concentration of hydrogen is relatively high for Cases I and II (0.2%) and significantly lower for Cases III and IV (0.016%). The average concentrations of the hydrogen atoms in the film for Cases III and IV are determined as 0.2 and 1.8%, respectively. This difference should be attributed to the effect of the substrate or film temperature (1073 K for Case III and 1500 K for Case IV).

The average concentrations of vacancies in the deposited film for the four cases are determined as follows: Case I, 0.8%; Case II, 0.1%; Case III, 0.3%; and Case IV, 1.4%. This finding suggests that the substrate temperature (1500 K for Cases I and IV and 1073 K for Cases II and III) has the largest effect on the concentration of vacancies in the deposited film.

The effect of process conditions on the atomic surface configuration and the film quality in general is further quantified by determining the roughness of the film surface. Two measures of roughness are used in the present work: the root mean square average (R_q) roughness defined as

$$R_q = \left(\left(\sum_{i=1}^{N} (z_i - C)^2 \Big/ N \right) \right)^{1/2} \tag{8}$$

and the maximum roughness height defined as

$$R_t = z_{\max} - z_{\min}, \tag{9}$$

where z_i is the z-coordinate of surface atom i, N the total number of surface atoms, $z_{\max}$ and $z_{\min}$ the z-coordinates of the atoms residing on the top of surface asperities and the ones at the bottom of surface valleys, and C is defined as

$$C = \sum_{i=1}^{N} z_i \Big/ N \tag{10}$$

The variation of the root mean square average and the maximum height roughness for the four cases analysed in the present work are shown in Fig. 9a and b, respectively. To help the interpretation of the results

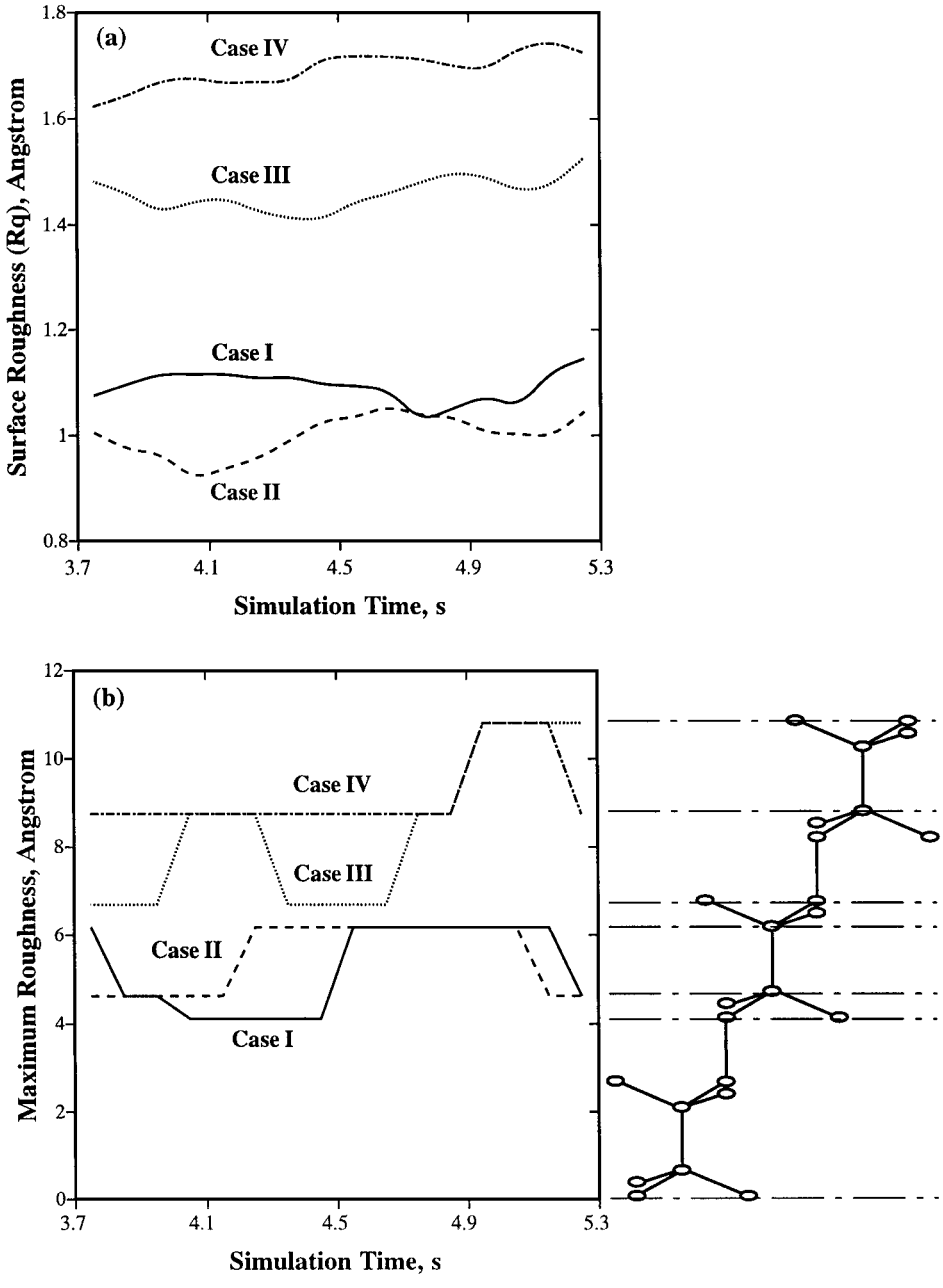

Figure 9 Variation of the mean root square average roughness (a) and maximum height roughness (b) with deposition time for the four cases analysed.

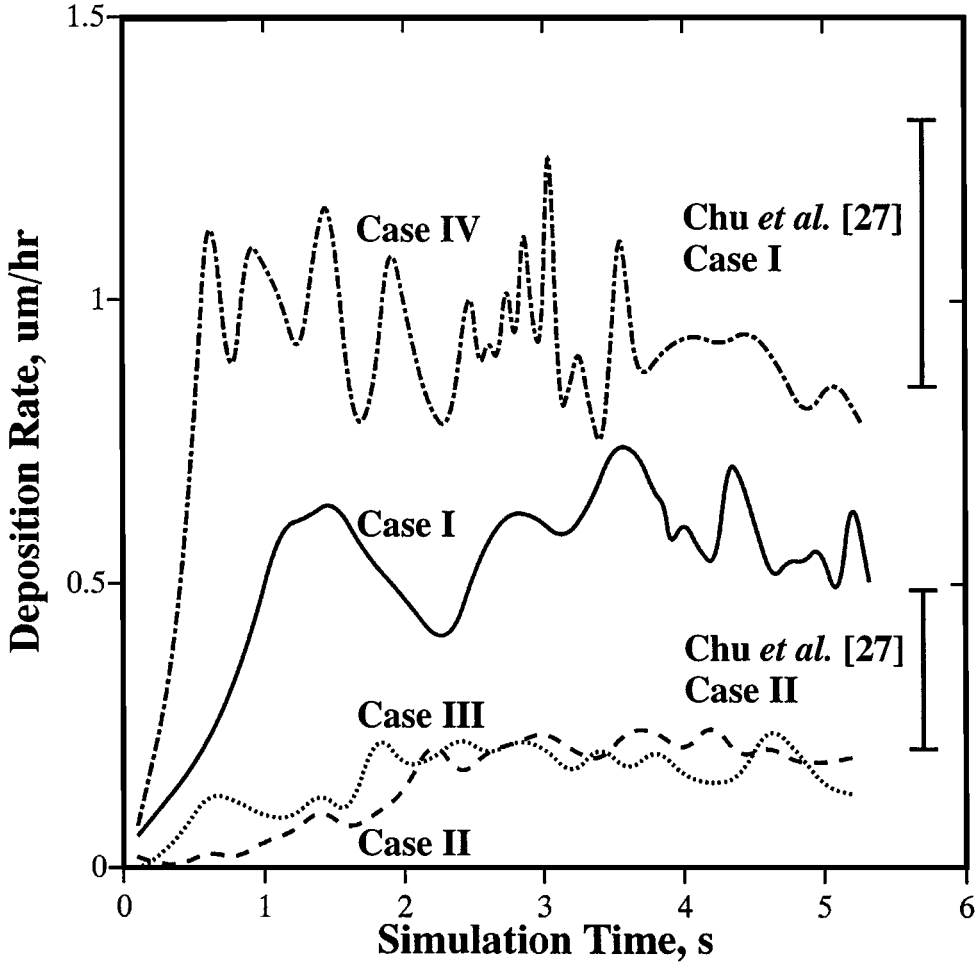

Figure 10 Variation of the film deposition rate with deposition time for the four cases on process parameters and the average deposition rates for Cases I and II as reported by Chu *et al*. [27].

shown in Fig. 9b, a schematic of the diamond crystal structure is included. The results shown in Fig. 9a and b show that both the substrate temperature and the feed gas chemical composition affect the surface roughness. For the same chemical composition of the feed gas, the higher the temperature, the higher the roughness (Case I versus Cases II and IV versus Case III). Also, the higher the concentration of CH_4 in the feed gas, the higher the roughness (Cases I and II versus Cases II and IV).

The effect of process parameters on the film deposition rate for the four cases analysed here is also examined. The film deposition rate is computed by dividing the product of the number of atoms deposited in a given time interval and the average (111) interplanar spacing by the product of the number of carbon atoms in a completely filled (111) layer and the time interval. The time interval of 0.1 s was used to compute the film deposition rate in the present work, and the results of this calculation are shown in Fig. 10. For comparison, the experimental results of Chu *et al*. [27] for the low CH_4 percentage cases (Cases I and II) are also given in Fig. 10.

In each of the four cases, the deposition rate is initially lower as the film deposition takes place on the substrate passivated by a larger amount of hydrogen. Once the film is in the third stage of deposition, the deposition rate oscillates around an average value. The average deposition rates for the four cases are assessed as follows: Case I, 0.60 μm/h, Case II, 0.20 μm/h, Case III, 0.21 μm/h, and Case IV, 0.95 μm/h. The deposition rate is thus not significantly affected by the chemical composition of the feed gas at lower temperatures (Case II versus Case III) but becomes quite sensitive to the feed gas chemical composition at high temperatures (Case III versus Case IV). The higher deposition rate for Case IV relative to Case I can be attributed to the higher concentration of CH_4 in the feed gas in the former. As far as the effect of substrate temperature on the deposition rate is concerned, it is significant for both chemical compositions of the feed gas analysed. High deposition rates achieved at high substrate temperatures (Case I versus Case II and Case IV versus Case III) confirm the thermally activated nature of surface chemical reactions. The activation energies calculated as $-(1/R)d \ln v_d/d(1/T)$, where v_d is the deposition rate, are found to be 8.3 kcal/mol for the two low CH_4 cases (Cases I and II) and 11.7 kcal/mol for the two high CH_4 cases (Cases III and IV). These values are consistent with the value of 12.0 kcal/mol obtained experimentally by Chu *et al*. [27].

4. Summary

A kinetic Monte Carlo program based on a transitional probability of one and a variable time increment is employed to study the deposition of (111)-oriented

diamond films at two substrate temperatures (1073 K and 1500 K) and two chemical compositions of the feed gas typical for a hot filament CVD process. The deposition rates obtained fall in a range between 0.1 to 1.0 μm/h, which is in general agreement with the one determined experimentally. The activation energies obtained fall into a range between 8.3 and 11.7 kcal/mol and are consistent with their experimental counterparts. The study shows that higher deposition rates are achieved by increasing the substrate temperature and the concentration of hydrocarbons (CH_4 in the present case) in the feed gas. The quality of the deposited film judged by the concentration of point defects (vacancies and hydrogen atoms embedded in the film) and by surface roughness, however, worsens as the deposition rate increases. Therefore, for each specific application of diamond films for which the maximum level of defects is specified, one can determine the appropriate substrate temperature and the feed gas chemistry that would result in a maximum deposition rate.

Acknowledgements

The work presented here has been supported by the U.S. Army Research Office, Grant DAAH04-96-1-0197, and the National Science Foundation under Grants DMR-9317804 and CMS-9531930. The authors are indebted to Dr Wilbur C. Simmons of ARO and Drs Bruce A. MacDonald and William A. Spitzig of NSF for the continuing interest in the present work. The authors also acknowledge the support of the Office of High Performance Computing Facilities at Clemson University.

References

1. K. E. SPEAR, *J. Amer. Ceram. Soc*. **72** (1989) 171.
2. J. E. BUTLER and R. L. WOODIN, *Philos. Trans. R. Soc. Lond. A* **342** (1993) 209.
3. D. G. GOODWIN and J. E. BUTLER, in "Handbook of Industrial Diamonds and Diamond Films," edited by M. A. Prelas, G. Popovici and L. K. Bigelow (Dekker, New York, 1997), pp. 527–582.
4. D. W. BRENNER, *Phys. Rev*. **B42** (1990) 9458.
5. B. J. GARRISON, E. J. DAWNKASKI, D. SRIVASTAVA and D. W. BRENNER, *Science* **255** (1992) 835.
6. D. HUANG and M. FRENKLACH, *J. Phys. Chem*. **96** (1992) 1868.
7. V. I. GAVRILENKO, *Phys. Rev. B* **47** (1993) 9556.
8. Y. L. YANG and M. P. D'EVENLYN, *J. Amer. Chem. Soc*. **114** (1992) 2796.
9. T. FRAUENHWIM, U. STEPHAN, P. BLAUDECK, D. POREZAG, H.-G. BUSMANN, W. ZIMMERMANN-EDLING and S. LAUER, *Phys. Rev. B* **48** (1993) 18189.
10. Z. JING and J. L. WHITTEN, *Surf. Sci*. **314** (1994) 300.
11. S. SKOKOV, C. S. CARMER, B. WEINER and M. FRENKLACH, *Phys. Rev. B* **49** (1994) 5662.
12. S. CIRACI and I. P. BATRA, *ibid*. **15** (1977) 3254.
13. S. F. YANG, D. A. DRABOLD and J. B. ADAMS, *ibid*. **48** (1993) 5261.
14. B. N. DAVIDSON and W. E. PICKETT, *ibid*. **49** (1994) 11253.
15. M. FRENKLACH and H. WANG, *ibid*. **43** (1991) 1520.
16. S. J. HARRIS and D. G. GOODWIN, *J. Phys. Chem*. **97** (1993) 23.
17. M. E. COLTRIN and D. S. DANDY, *J. Appl. Phys*. **74** (1993) 5803.
18. D. S. DANDY and M. E. COLTRIN, *J. Mater. Res*. **10** (1995) 1993.
19. M. M. CLARK, L. M. RAFF and H. L. SCOTT, *Comput. Phys*. **10** (1996) 584.
20. E. J. DAWNKASKI, D. SRIVASTAVA and B. J. GARRISON, *J. Chem. Phys*. **104** (1996) 5997.
21. C. C. BATTAILE, D. J. SROLOVITZ and J. E. BUTLER, *Diamond Relat. Mater*. **6** (1991) 1198.
22. *Idem, J. Appl. Phys*. **82** (1997) 6293–6300.
23. SURFACE CHEMKIN III User Manual, Sandia National Laboratories, San Diego, CA, 1996.
24. D. S. DANDY and M. E. COLTRIN, *J. Appl. Phys*. **76** (1994) 3102.
25. M. GRUJICIC, S. G. LAI and P. GUMBSCH, *Materials Science and Engineering* **A231** (1997) 151–162.
26. R. FLETCHER and C. M. REEVES, *Comput. J*. **7** (1964) 149.
27. C. J. CHU, R. H. HAUGE, J. L. MARGRAVE and M. P. D'EVELYN, *Appl. Phys. Lett*. **61** (1992) 1393.

Received 30 July
and accepted 31 July 1998